Geomorphology 235 (2015) 63–76

Contents lists available at ScienceDirect

Geomorphology

journal homepage: www.elsevier.com/locate/geomorph

Evaluating knickpoint recession along an active fault for paleoseismological analysis: The Huoshan Piedmont, Eastern China

Zhanyu Wei [a], Lisi Bi [b], Yueren Xu [c], Honglin He [a,*]

[a] Key Laboratory of Active Tectonics and Volcano, Institute of Geology, China Earthquake Administration, Beijing 100029, China
[b] Key Laboratory of Earthquake Monitoring and Disaster Mitigation Technology, Guangdong Provincial Earthquake Bureau, Guangzhou 100717, China
[c] Institute of Earthquake Science, China Earthquake Administration, Beijing 100010, China

ARTICLE INFO

Article history:
Received 27 June 2014
Received in revised form 9 January 2015
Accepted 18 January 2015
Available online 10 February 2015

Keywords:
Knickpoint
Paleoearthquake
DEM
Huoshan Piedmont Fault
Shanxi Faulted Basin zone

ABSTRACT

Ground-rupturing earthquakes can generate tectonic knickpoints within upstream reaches of streams across active fault zones. These knickpoints are characteristic of upstream propagation of time-related process once generated by an earthquake, so analysis of knickpoint series in streams which cross fault zones can be used to infer paleoearthquake events. We studied the knickpoints along the Huoshan Piedmont Fault (HPF), which is an active normal fault in the Shanxi Faulted Basin zone, China, and demonstrate that analysis of knickpoints shows evidence for two paleoearthquakes in the HPF. First, we identified knickpoints in bedrock reaches upstream of the HPF using high-resolution DEMs derived from IRS-P5 stereo images and the stream-gradient method. After excluding non-faulting knickpoints, 47 knickpoints were identified in 23 bedrock reaches upstream from the HPF. Analysis of the most recent knickpoints caused by the 1303 CE Hongdong Earthquake allowed for local calibration of the retreat rates. Applying these retreat rates across the study area allows for the estimation of the age of other knickpoints, and constrains the age ranges of two knickpoint groups to be 2269–3336 a BP and 4504–5618 a BP. These ages constrain the ages of two paleoearthquake events at 2710 ± 102 and 4980 ± 646 a BP. The knickpoints along the HPF obey the parallel retreating model in which knickpoint morphology was roughly maintained during retreat, so the heights of knickpoints represent the coseismic vertical displacements generated by the earthquakes along the HPF. The vertical offsets for these three earthquake events are similar and are approximately 4 m, which indicates that the ruptures on the HPF obey a characteristic slip model with a similar slip distribution for several successive earthquakes. These results provide additional evidence of paleoearthquakes on the HPF and show that analysis of knickpoint recession along an active fault is a valuable tool for paleoseismology.

1. Introduction

A complete record of large and destructive earthquakes is vital to accurately assess the potential seismic risk of an active fault and may even apply to earthquake forecasting (Wallace, 1981; Liu-Zeng et al., 2006; Klinger et al, 2011). We often lack sufficiently long historical or instrumental seismic data sets for such analysis because recurrence of large earthquakes along the same fault segment typically takes several hundred years or more (Scholz, 2002). Though trenching is one of the primary methods used in paleoseismology and has achieved outstanding results (Sieh, 1978; Liu-Zeng et al., 2006), geologists are often troubled by a lack of sufficient material to determine the date of past earthquakes in a trench. Moreover, trenching cannot be applied in bedrock sites and has shortcomings in acquiring the coseismic displacements along faults.

If an earthquake is large enough to disrupt and displace geological and geomorphic units, the event date, size, and rupture process may be preserved in the geologic and geomorphic record (Burbank and Anderson, 2001). One earthquake can produce various landforms, such as troughs, sags, scarps, and offset channels along the fault zone (Wallance, 1968; Arrowsmith and Zielke, 2009). To obtain seismic records sufficiently extensive to span multiple earthquake cycles, or to reconstruct the coseismic displacement, geologists can use these tectonic landforms as markers, such as offset channels or terrace edges where strike–slip faulting took place (Wallance, 1968; Sieh and Jahns, 1984; Klinger et al, 2011), bedrock scarps where normal faulting took place (Stewart, 1996; Giaccio et al., 2002), and fault scarps in unconsolidated sediments where thrust faulting and normal faulting took place (Nash, 1980; Andrews and Hanks, 1985; Arrowsmith et al., 1998), and combining these with the radiocarbon dating of organic matter associated with the displaced deposits allows for age calibration (Scholz, 2002; McCalpin, 2009).

Knickpoints are important geomorphologic features in the longitudinal profiles of bedrock rivers, and can be generated by the base-level changes produced by an increase in the rate of rock-uplift (Whittaker et al., 2008; Attal et al., 2011) or eustatic adjustment (Whipple and

* Corresponding author.
E-mail address: honglinhe123@vip.sina.com (H. He).

http://dx.doi.org/10.1016/j.geomorph.2015.01.013
0169-555X/

Tucker, 1999; Snyder et al., 2003; Bishop et al., 2005). Base-level fall knickpoints have been observed in a range of tectonic settings (Loget and van den Driessche, 2009), and can give insight into geomorphological erosional mechanisms (Gardner, 1983) and landscape evolution (Righter, 1997; Bishop et al., 2005; Crosby and Whipple, 2006; Foster and Kelsey, 2012). We are more interested in tectonically generated knickpoints, formed by differential faulting across rivers. Normal or thrust faulting lowers the base level of erosion (with respect to the upstream segment of the river) across the fault (Burbank and Anderson, 2001). In this case, one knickpoint (a fault scarp in the reach of a river) develops in the longitudinal profile of river, especially in bedrock-dominated channels (Hayakawa and Oguchi, 2006; Ming-Chu, 2010). Knickpoints characteristically migrate upstream over time, and their age of formation can be calculated by dividing retreat distances by retreat rates. In many tectonically active regions, multiple knickpoints within a reach of river upstream from a fault zone may indicate that there have been multiple surface-rupturing earthquakes. However, it has seldom been considered as a useful geomorphic marker for the investigation of repeated surface faulting. Investigating knickpoint characteristics and spatial distribution commonly relies on exhaustive surveys and the interpretation of aerial photography. Therefore, a highly effective method is required to carry out an investigation of the geomorphology of knickpoints and their spatial

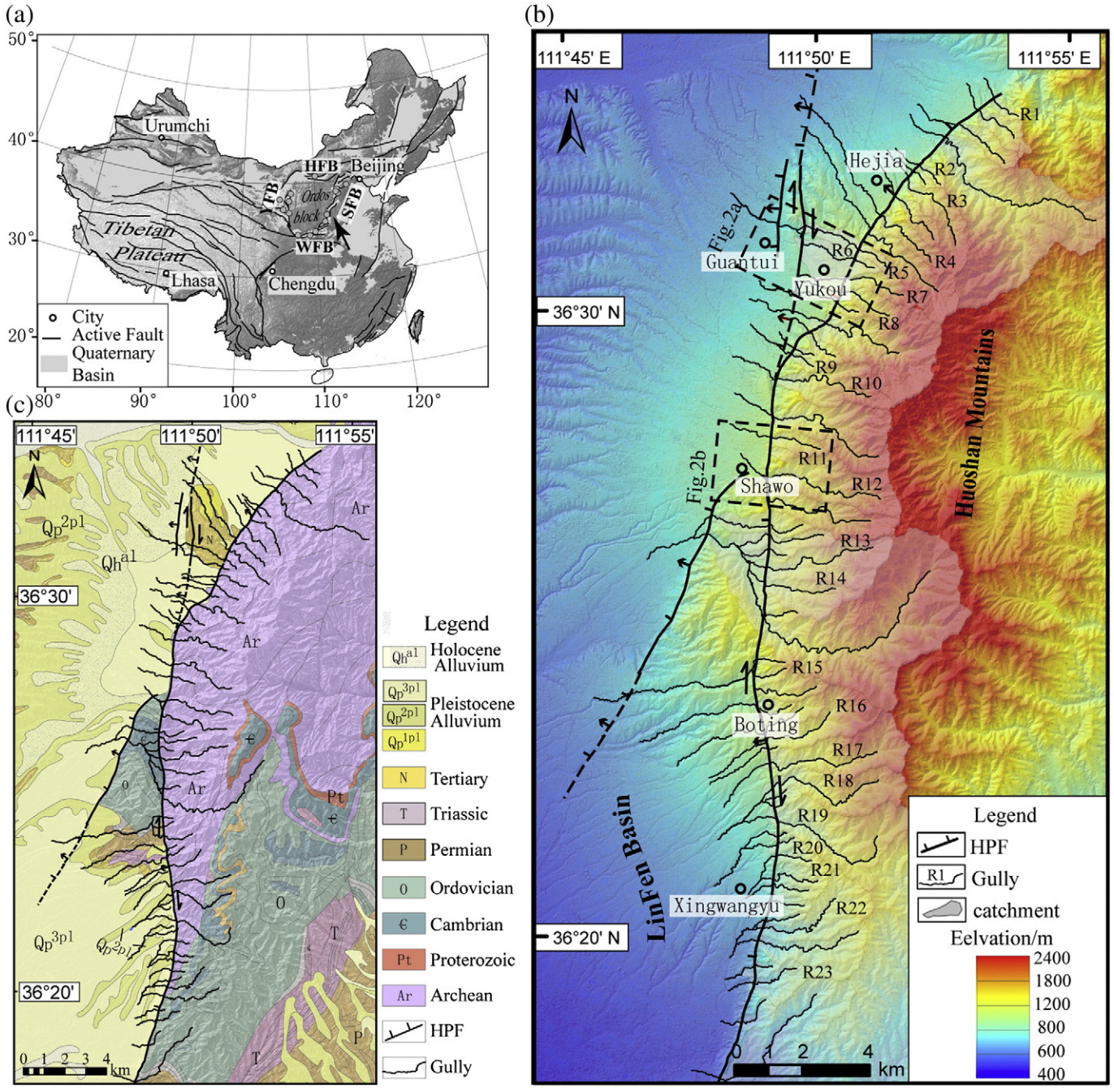

Fig. 1. Simplified map of the tectonic setting of China, and the topographic and geologic maps of the Huoshan Piedmont Fault (HPF). (a) Major active faults of China (modified from Qidong et al., 2007), black lines indicate active faults; the black arrow shows the location of (b). (b) Topographic map and the HPF. Thick black lines indicate the HPF and thin black lines indicate streams; R*x* marks the streams which are studied here; the base map is from DEMs with a horizontal resolution of 2.5 m in a UTM projection, generated from six IRS-P5 stereo images. (c) Geologic map along the HPF. Black lines are the same as (b).

distribution. Recent developments in high-resolution digital elevation models (DEMs) and mathematical models to identify knickpoints (or knickzones) such as slope–area relationships based on the stream power erosion model (Howard and Kerby, 1983; Bishop et.al., 2005; Zhang et.al., 2011), and stream gradient calculations (Hayakawa and Oguchi, 2006, 2009) have enabled detailed analysis of knickpoints, allowing these knickpoints to provide a basis for subsequent paleoseismic analysis.

In this paper, we report observations of knickpoints from the 60-km-long Huoshan Piedmont Fault zone (HPF), one of the boundary faults of the Shanxi Faulted Basin zones (SFB), China (Fig. 1a). Here, abundant knickpoints in rivers that cross this fault zone allow us to construct a detailed time series of earthquakes caused by normal faulting, and the response of erosional processes and topography to the base-level changes along reaches of the river. Detailed geologic and geomorphic field observations based on aerial interpretation constrain the location of faults, and recently acquired IRS-P5 stereo images provide high-resolution topographic data. These data provide an excellent opportunity for paleoseismology using the detailed distribution of knickpoints along the fault zone. First, we introduce a method to identify knickpoints where steepened slopes of reaches are sufficiently anomalous. Second, we exclude all other knickpoints unrelated to the earthquake faulting before the paleoseismic analysis. Finally, we discuss paleo-earthquakes on the target fault based on the normalised distribution of knickpoints and knickpoint attributes (in general, the scarp height).

2. Study area

2.1. Geological structure

As an important transitional region adjacent to the Tibetan Plateau, the Ordos block bridges the intensively uplifted Plateau and the disassembled old North China Craton (Deng et al., 1999; Wang et al., 2011) (Fig. 1a). Due to compressional stress from the movement of the Tibetan Plateau towards the Northeast, four fault zones (and corresponding faulted basin zones) have developed sequentially in Cenozoic lithologies surrounding the Ordos block (Xu and Ma, 1992; Deng and Xu, 1994, 1999). The Weihe Faulted Basin zone (WFB) and Yinchuan Faulted Basin zone (YFB) to the south and west initiated during the Eocene, followed by the Hetao Faulted Basin zone (HFB) to the north in the Oligocene, and finally, the Shanxi Faulted Basin zone (SFB) to the east in the Pliocene. Compared to the stable Ordos block, these faulted basin zones are characterised by high seismicity (Xu and Ma, 1992; Deng et al, 1999).

The Huoshan Piedmont Fault zone (HPF) is an important active normal fault in the Shanxi Faulted Basin zone, and is the dominant control on the development of the Linfen Basin (Fig. 1b). Field investigations show that the HPF is a 60-km long, N10°–N20° trending active fault, with a simple geometric structure (Xu and Ma, 1992). Bedrock fault planes and multiple fault facets exposed along the HPF separate the bedrock of the mountain to the east from the faulted basin to the west (Figs. 1b and 2), and indicate major normal faulting with a minor sinistral strike–slip component. The geology of Mt. Huoshan in the east is dominated by an anticline, the core of which consists of Archean gneiss, and its east and west flanks are Palaeozoic limestone. The faulted basin to the west mostly consists of alluvial deposits overlying loess strata of Pliocene age and younger (Fig. 1c). Detailed mapping of the HPF was carried out through a field survey and aerial-photo interpretation (Xu et al., 2011).

2.2. Present landscape morphology

In the study area there are many rivers with catchment sizes less than 1 km^2 flowing westward and across the HPF (Figs. 1 and 2). Most of these rivers have deeply incised upstream reaches on the upthrown fault block, along which many knickpoints have been generated (Fig. 3). Numerous knickpoints provide an opportunity to identify repeated faulting on the HPF. Except for those produced by non-tectonic causes, such as lithological differences, and climate, knickpoints caused by normal faulting can be used as a geomorphic indicator of repeated surface rupturing earthquakes.

The climate of the study area is semi-arid with a mean annual temperature ranging from 8.9–12.1 °C. The annual precipitation ranges from 400–500 mm, most of which occurs in summer and fall. The Huoshan Mountains lie below 2000 m in elevation. We did not find any glacial landforms along the HPF during our field surveys, consistent with other previous survey reports (Xu et al., 1993; Deng et al., 1994).

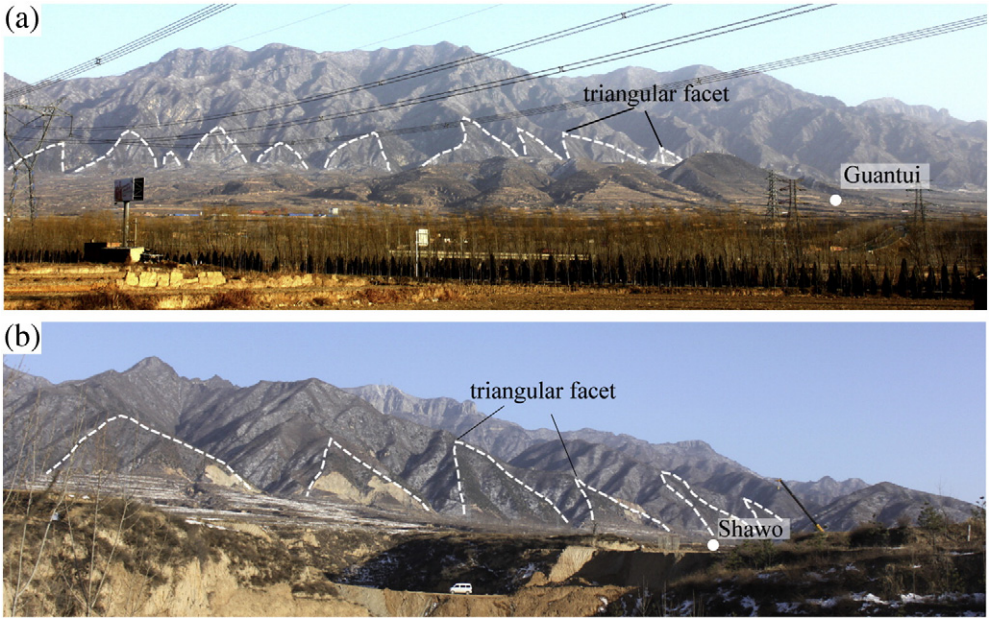

Fig. 2. Panoramic views of tectonic landforms along the HPF from the Linfen Basin, looking east. White dashed lines delineate the triangular facets of the HPF. The location of (a) and (b) is shown in Fig. 1b.

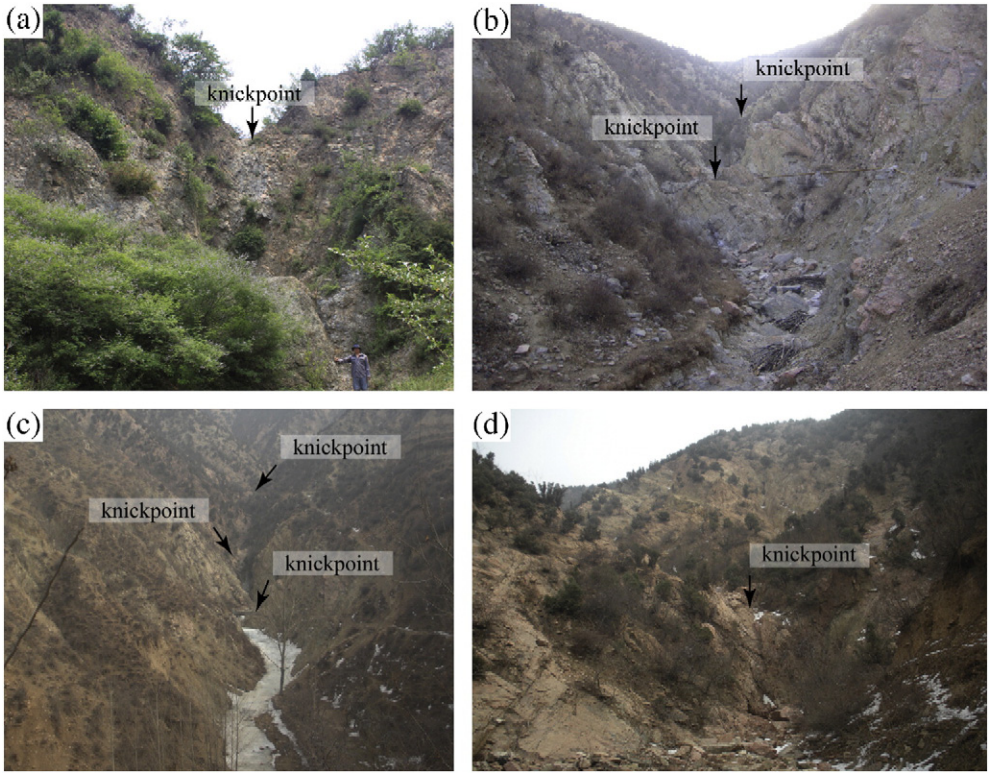

Fig. 3. Photos of knickpoints located in upstream channels that cross the HPF. Observed knickpoints in (a), (b), (c) and (d) are from profiles R21, R13, R17 and R18, respectively.

Geologists have concluded that the mid-low mountains (altitude < 3000 m) in eastern China were not glaciated during the last glacial maximum (Jijun, 1988; Yafeng, 1989).

2.3. Earthquake history

The late Quaternary geological history of the HPF has been well studied (Xu and Deng, 1990; Deng and Xu, 1994; Yueren et al., 2011). Historical earthquake analyses and paleoseismic investigations along the HPF indicate that multiple ground-rupturing earthquakes occurred during the Holocene (Xu and Deng, 1990; Xu et al., 1993). The most recent surface-rupturing earthquake, recorded in historical documents, is the Hongdong Earthquake with an estimated magnitude of *M*8 in 1303CE. Based on air photo interpretation and field observations, Xu and Deng (1990) identified an approximately 45 km long surface rupture caused by the 1303 CE earthquake. This interpretation used various tectonic geomorphic features, such as fault scarps, offset streams, and landslides. Systematic measurements of these offset geomorphic features have led to an understanding of the coseismic slip distribution, with a vertical displacement of up to 5 m during the 1303 earthquake (Jiang et al., 2004).

Paleo-seismologic analysis of trenches and dating of calibrated radiocarbon indicate that other than the Hongdong Earthquake of 1303, there were two other paleo-seismic events along the HPF in the Holocene. The earlier earthquake event has been dated at approximately 5455 ~ 4620 a BP, and the second event at approximately 3475 ~ 2555 a BP (Xiwei et al., 1993). Recent research has indicated that the average recurrence interval for surface faulting events is between 1500 and 2000 years (Wali et al., 2004).

3. DEMs and stream profile extraction

This study uses DEMs with a horizontal resolution of 2.5 m in a UTM projection (Fig. 1b). The DEMs were generated from six IRS-P5 stereo images, which cover the entire study area. Every stereo image consists of a set of overlapping satellite images (a forward image and a rear image). We used digital photogrammetric software to generate the DEMs. We used the calibration information of the stereo images, along with 12 ground control points acquired from a centimetre-accurate differential GPS, to help calibrate the DEMs. We tested the quality of the DEMs using the contour overlap analysis method with the contour data of 1:50,000 topographic maps with a 20-m vertical resolution published by the National Geomatics Centre of China. This comparison shows that the DEMs agree well with topographic maps in all dimensions and landform shapes (Fig. 4).

Longitudinal profiles of the streams crossing the HPF were extracted utilising River Tools Software which is an application for digital terrain and river network analysis. After sinks in the original DEMs were filled, water flow direction, drainage area, and stream network models were created from the filled DEMs (Jenson and Domingue, 1988). Longitudinal profiles of some streams were made with a differential GPS to verify the accuracy of the DEM-derived profiles. The DEM-derived river profiles were systematically higher than the field measured profiles because the elevations generated from the photogrammetric techniques are affected by adjacent valley-side slopes (Hayakawa and Oguchi, 2006). These results show that the presence and location of knickpoints observed on DEMs are consistent with those derived from field measurements, and that the relative elevation errors are less than 1 m (Fig. 5). This shows that the DEMs derived from IRS-P5 stereo images meet the accuracy requirements needed to identify knickpoints (Guo-an et al., 2005; Liping et al., 2007).

The area of drainage basins above the intersection of the fault and the channel can be determined using the DEM. Streams with large drainage areas (>1 km^2) have high erosion power and transport huge boulders. This makes it difficult to identify knickpoints in longitudinal profiles of large drainage basins because of the large number of boulders in the riverbed. Therefore, in this study we focus on small streams with drainage areas of less than 1 km^2 above the intersection of the fault and the stream. In addition, streams in which there are man-made dams are excluded.

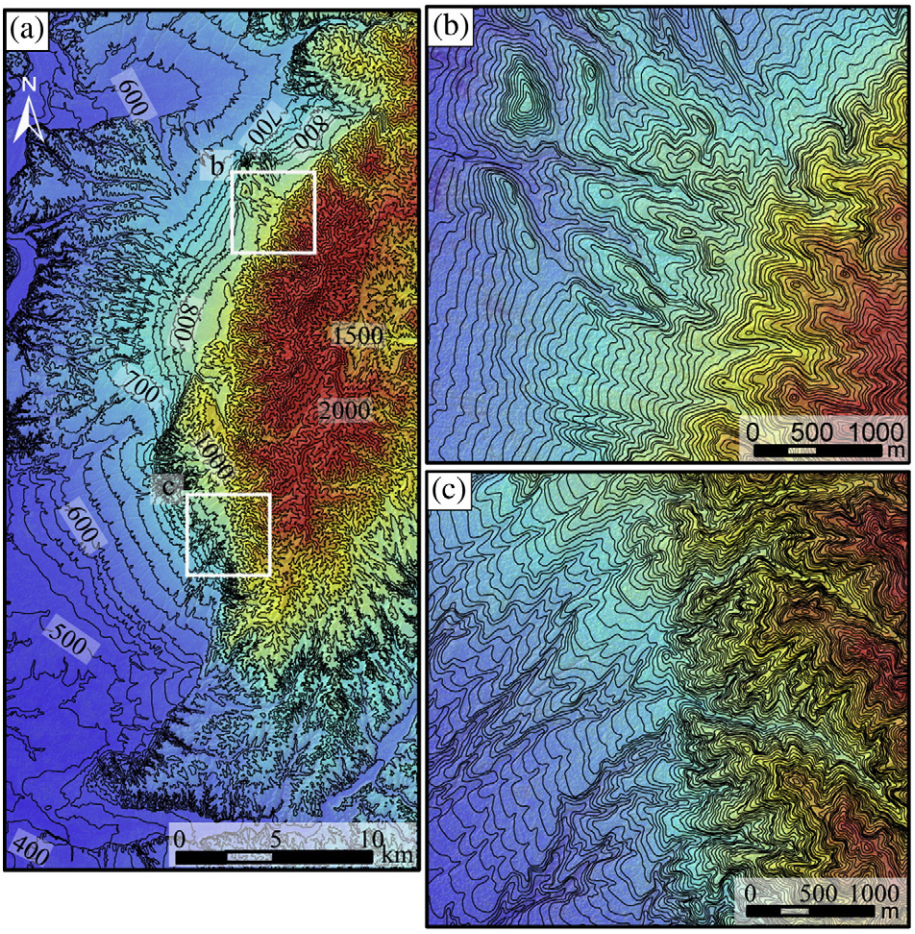

Fig. 4. Assessment of the accuracy of DEMs generated from IRS-P5 stereo images by the contour overlap analysis method. (a) Comparison of DEM data (base map) and 1:50,000 topographic maps (contour data) published by National Geomatics Centre of China. White rectangles indicate the locations of (b) and (c). (b) and (c) are enlarged views of the topographic section delineated by the white boxes in (a). The comparison shows that DEM agrees with topographic maps in terms of magnitude and geometry.

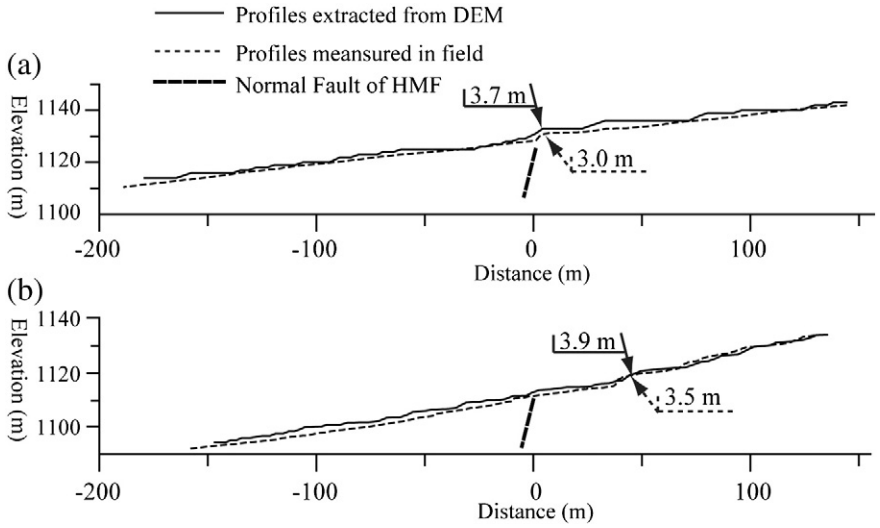

Fig. 5. Comparisons between the profiles extracted from DEMs and the profiles acquired from field measurement at the same locations. Numbers indicate the heights of knickpoint scarps measured from the DEM and from field measurements. (a) Knickpoint is close to the fault zone (R16, Fig. 9). (b) Knickpoint has migrated upstream, away from the fault zone indicated by dashed thick line (R17, Fig. 9).

4. Method

4.1. Paleo-earthquake analysis based on knickpoint series

Down-faulted blocks can initiate an upstream-propagating wave of incision in river reaches that cross the fault zone (Gardner, 1983; Hayakawa et al., 2010; Whittaker et al., 2010). Such migrating incision can take the form of transitory knickpoints (or knickzones) in the longitudinal profile of a riverbed (Crosby and Whipple, 2006; Wobus et al., 2006). We use a simple model of knickpoint formation and recession to build the conceptual model for the geomorphic processes observed in this study (Fig. 6). Previous studies have shown that river profiles are assumed to display a sustained decrease in channel slope in a downstream direction under conditions of steady rock uplift and invariant lithology (Burbank and Anderson, 2001), and are usually characterised by a concave up smooth curve in numerical modelling studies (Duvall et al., 2004; Whipple, 2004; Attal et al., 2011). We used a concave up smooth curve to model the original longitudinal profile of a river that crosses a fault zone. A ground-rupturing earthquake that vertically displaces the longitudinal profile generates a knickpoint (P1) in the river where it crosses the fault. Subsequently this knickpoint (P1) migrates upstream at some rate due to continuous retrogressive erosion. When further ground-rupturing earthquakes occur, the geomorphic process described above repeats itself. A new knickpoint (P2) is generated, and the old knickpoint (P1) migrates upstream a certain distance from the fault zone along the river reach. Both old and new knickpoints (P1 and P2) continue to migrate upstream due to retrogressive erosion. Therefore, multiple earthquakes attributed to normal faulting can create multiple knickpoints (P1, P2, P3…) in rivers that cross an active fault zone. The number of knickpoints distributed in river reaches not only indicates the number of faulting events, but the distance between adjacent knickpoints can imply the time interval between two faulting events.

We can create an earthquake record for an active fault based on the following two hypotheses. (1) The knickpoints migrate upstream at a constant rate since they were formed, and the retreat rates of knickpoints within the same river are equal. In reality, the retreat rate of a knickpoint would be affected by changes in the drainage area. The drainage area decreases as a knickpoint migrates upstream. For the streams in the Huoshan Mountains, the majority of the drainage area is usually located in the headwaters of the streams, and the knickpoints caused by faulting are located in the lower reaches of the streams. Because of this, there is little difference in the drainage area among knickpoints in the same channel. (2) The formation time of the most recent knickpoint (P_n) is known from historical data or a trench study, and the retreat distances of all of the other knickpoints from the active fault zone along the channel can be determined.

First, we can calculate the retreat rate of the knickpoint of each stream with the following formula:

$$v = L_N / T_N \tag{1}$$

where v is the retreat rate of a knickpoint, L_N is the retreat distance, and T_N is the formation time of the most recent knickpoint.

Second, the formation times, T_i, of other knickpoints can be estimated by the formula:

$$T_i = L_i / v \qquad i = 1, 2, \ldots\ldots, N-1 \tag{2}$$

where L_i is the retreat distance of the knickpoint determined by measuring the streamwise distance from the active fault zone. Because the knickpoints mentioned above are all assumed to be produced by multiple normal faulting events, the formation time of every knickpoint implies the occurrence time of a surface-rupturing earthquake. Through statistical analysis of knickpoint distribution in rivers that cross an active fault zone, the paleo-earthquake record of the active fault can be determined.

4.2. Identification of knickpoints based on DEMs

A knickzone is a locally high-gradient reach between lower gradient reaches in a river. The knickpoint associated with a knickzone is located at the distinct inflection point between a knickzone and an upstream, lower gradient reach (Crosby and Whipple, 2006; Wobus et al., 2006). We employed the stream-gradient method described by Hayakawa and Oguchi (2006, 2009) to identify knickpoints in the riverbed. Stream gradients of rivers are first computed with varying measurement lengths, and then an index of relative steepness is derived from the stream gradients in order to determine the location of knickpoints with more quantitative rigour than visual inspection (Fig. 7).

The longitudinal profiles of the study streams were sampled at a 3.5 m interval, equal to the diagonal length of a grid cell, and a 15 m smoothing window was applied to each stream profile. A smoothed profile is a better representation of the true channel bottom observed in the field because the raw profiles include numerous small pits and features that may represent large woody debris in channels (Foster and Kelsey, 2012), or elevations of valley-side slopes (Hayakawa and Oguchi, 2006). Next, the gradient along the streams, G_d (m/m), was calculated for each sampling point with a measurement length of d (m):

$$G_d = \frac{e_2 - e_1}{d} \tag{3}$$

where e_1 and e_2 are the riverbed elevations (m) at $d/2$ upstream and downstream of the measurement point respectively (Fig. 7a).

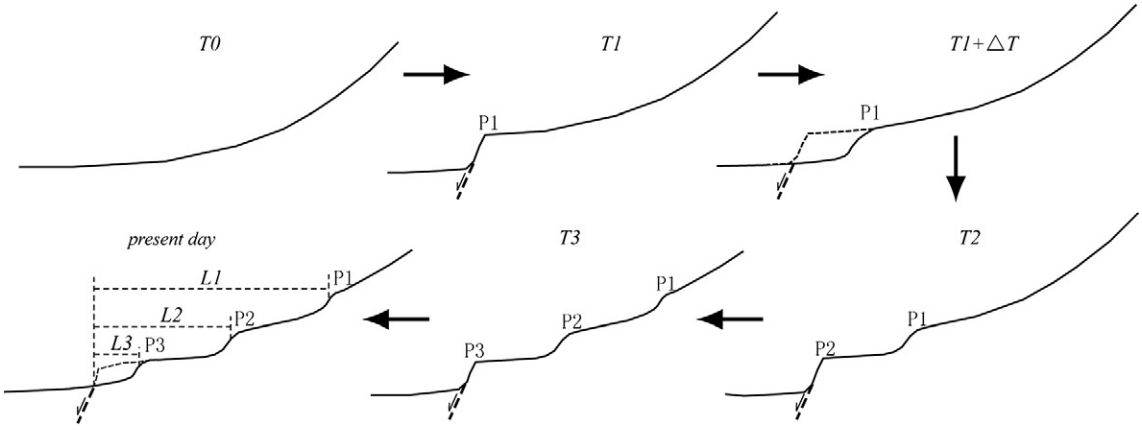

Fig. 6. Schematic illustration of development and upstream migration of fault-scarp knickpoints associated with normal faulting. P1, P2, and P3 represent different knickpoints caused by normal faulting; *T*0, *T*1, *T*2, and *T*3 are the times of earthquakes/knickpoint initiation; *L*1, *L*2, and *L*3 are recession distances from the fault zone. Dashed line indicates fault.

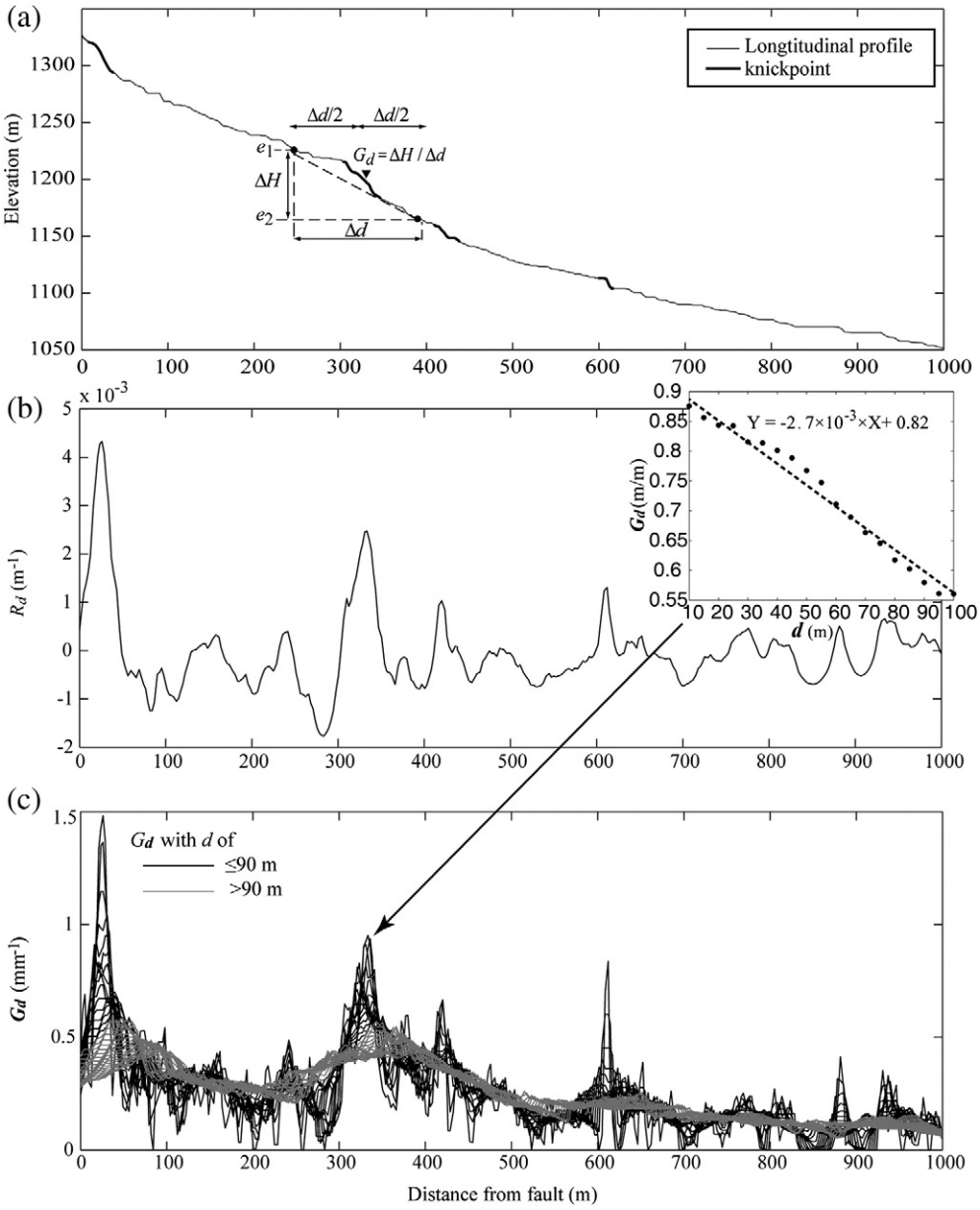

Fig. 7. Detection of knickpoints using the stream gradient method (Hayakawa and Oguchi, 2006). (a) Stream longitudinal profile (R2, Fig. 9) and location of identified knickpoints; G_d is stream gradient in the center point, e_1 and e_2 are elevation values at $\Delta d/2$ upstream and downstream points, respectively. (b) Knickpoints were extracted by interpreting the longitudinal changes (R_d) plot, with higher values of R_d identified as knickpoints. Inset figure shows a regression line (dashed) between G_d and Δd, and R_d is the negative slope of the regression line. (c) Longitudinal changes in gradient along the streams using different values for Δd.

For each sampling point, different G_d values can be obtained with different measurement lengths of d (Fig. 7c). G_d changes as a function of d according to the local riverbed morphology. By analysing the gradients of river profiles, a local gradient feature can be best reflected in G_d when d = 15–20 m, whereas the range of d from 20–95 m can be regarded as a transition from local to larger scale gradients. To quantify the transition for each measurement point, a regression line is fitted to the relationship between G_d and d, within a d range of 15–95 m at 5 m intervals:

$$G_d = -R_d \times d + b \tag{4}$$

where R_d and b are coefficients of the linear regression. R_d is defined as the negative slope coefficient of the regression line, and represents how the local gradient of the measurement point is steeper than its trend gradient. An example of R_d distribution along a river is shown in Fig. 7b, where the curve of R_d along the river shows fluctuations, in which locally steep knickzones can be regarded as river segments with large R_d values. However, we did not use a threshold value of R_d to automatically identify knickzones, such as Hayakawa and Oguchi (2006) did, because we found that it is difficult to determine a threshold value to objectively define the knickzones in longitudinal profiles of streams with a small drainage area (<1 km^2). Instead, we used visual interpretation to locate the knickpoints by referring to the obvious peaks observed in the G_d–d relation coupled with detailed individual analysis of longitudinal stream profiles. Then the height of individual knickpoints was simply determined as the vertical distance between the upstream and downstream sides of the knickzone.

4.3. Determination of knickpoints caused by faulting

The knickpoints obtained by the method mentioned above include not only knickpoints caused by faulting but also false knickpoints caused by data noise, and other types of knickpoints generated by

differences in local lithology or inflow from tributaries. This makes it necessary to exclude non-faulting knickpoints before beginning the paleo-earthquake analysis.

We only examined knickpoints located in river reaches on the footwall of a fault, as the knickpoints caused by normal faulting only exist on the footwall. We first performed visual inspections of every longitudinal stream profile on which knickpoints are identified. If the reach near a knickpoint shows frequent elevation fluctuations, we consider such knickpoints as singular points caused by data noise in longitudinal profiles. Otherwise, if the reach near a knickpoint shows a smoothly concave upward profile, we conclude that such a knickpoint may be generated by natural factors.

In addition to inspection of longitudinal profiles, we also carefully analysed the spatial relationship between knickpoint locations and lithologies, tributary junctions and the turning points of each river. These factors can usually produce knickpoints in bedrock rivers (Wohl, 1993). To do this, we compared knickpoint locations with geologic and topographic maps (Fig. 8). The knickpoints are excluded if they occur at lithologic contacts, the confluence of tributaries and/or a bend in the river. Such knickpoints are relatively tall and steep.

Using some empirical relationships between moment magnitude, surface rupture length, and surface displacement (Qidang et al., 1992, Wells and Coppersmith, 1994), an earthquake with moment magnitude $M = 7.0–8.0$ is likely typical for the HPF based on the length of the fault system, and such an earthquake could generate a fault scarp of 4–10 m in height. Through field investigations of the HPF, and statistics of surface ruptures for the historic M 8.0 earthquake in 1303 CE, the vertical surface displacement from this earthquake is approximately 5 m (Xiwei et al., 1993). Therefore, a threshold value was used to identify whether faulting caused a knickpoint. Knickpoints higher than 10 m are considered to be non-faulting knickpoints in this study, and were not included as knickpoints in the paleoseismic analysis.

To verify the reliability of the method of knickpoint identification mentioned above, some of these knickpoint locations were visited during the differential GPS field surveys. These knickpoints were confirmed easily in the field because they usually have a relatively steep face and some even form small waterfalls, especially knickpoints occurring in erosion-resistant rocks. This fieldwork confirmed the suitability of the identification method for knickpoints based on DEMs.

5. Results

5.1. Selected longitudinal profiles and knickpoints

We examined 69 profiles of streams that cross the HPF, and more than 80 knickpoints were identified in bedrock reaches. Two types of river reaches were excluded. One type of reaches did not have any knickpoints. Such reaches are useless for analysing the paleo-earthquake sequence. The other type of reaches had frequent knickpoints. We think these knickpoints could be caused by data noise from the extracted longitudinal profiles. We ultimately selected 23 bedrock reaches, and from these 47 knickpoints were filtered out to remove those that were unlikely to be earthquake generated, as discussed in Section 4.3.

5.2. Characteristics of knickpoints

Abundant knickpoints were found in the streams crossing the HPF in the footwall during field surveys. Our observations show that these knickpoints usually maintain a steep face (Figs. 3 and 9), but are somewhat different in height. Most of these knickpoints are 3–6 m high, but some knickpoints are more than 10 m and are often composed of one or two near-vertical drops (Fig. 3a).

All knickpoints are located less than 500 m upstream from the HPF. According to the number of knickpoints, the 23 bedrock reaches are divided into three classes (Fig. 10, Table 1). Class I reaches including R4, R7, R9, R16, and R21 only developed one knickpoint, and these knickpoints are close to the HPF zone and usually have a relatively steep scarp with a height of 4.0–7.5 m. Class II reaches including R6 and R15 developed two knickpoints. In these reaches, the most recent knickpoints are close to the HPF zone, and the heights are 4.5–6.0 m, similar to knickpoints in Class I reaches. We suspect that the knickpoints in reaches of Classes I and II have not significantly migrated upstream since they were formed. These knickpoints have a relatively high and steep scarp due to the superimposed vertical displacements of more than one earthquake. Class III reaches include another 16 reaches which developed 2–3 knickpoints with heights between 2.0 and 5.5 m. Among the knickpoints in Class III reaches, the most recent (level 1) knickpoints have retreated 40–70 m upstream with a mean

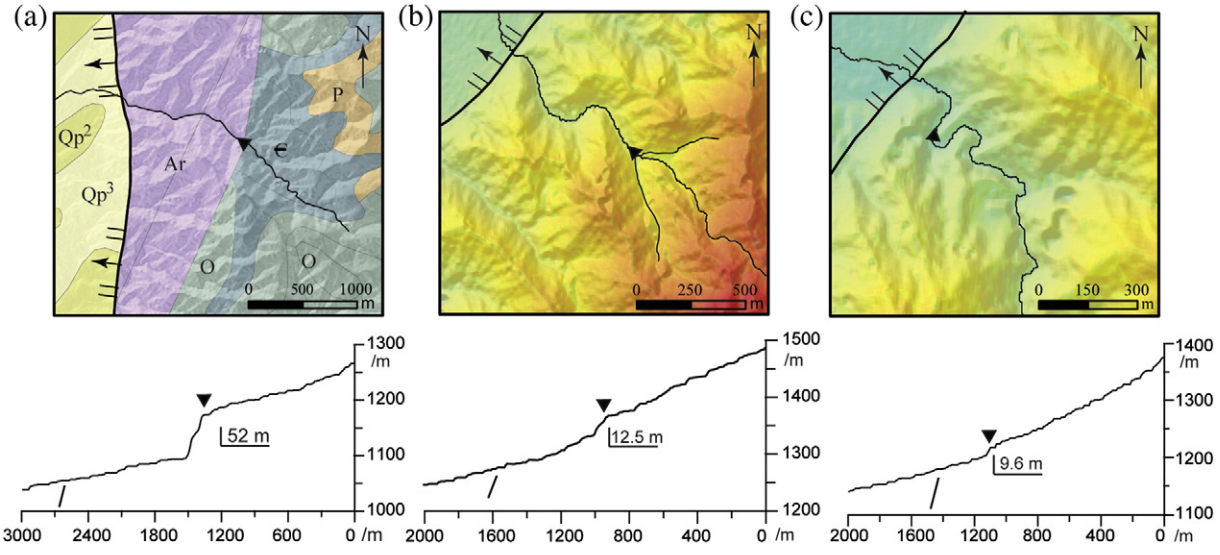

Fig. 8. Knickpoints located at positions of (a) lithology change, (b) tributary inflow, and (c) a bend of stream. Basemaps are geologic or topographic maps; thick lines with arrows indicate the HPF; thin line indicates streams crossing the HPF; and triangles indicate the locations of knickpoints. The lower plots are longitudinal profiles of streams across the HPF; the numbers indicate the heights of knickpoints.

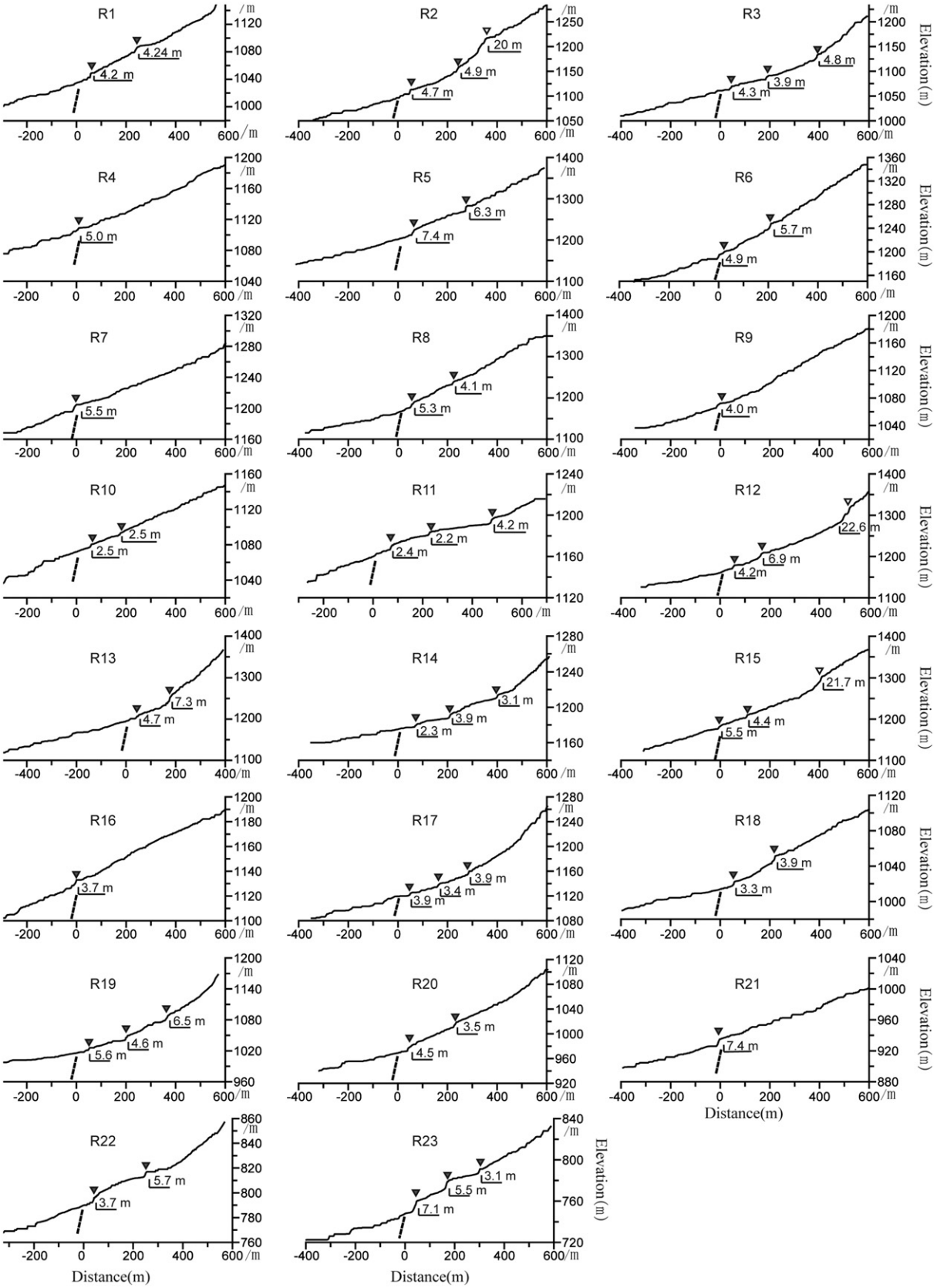

Fig. 9. Longitudinal profiles of streams with knickpoints, and the positions and heights of the knickpoint scarps. Dashed lines indicate the location of the HPF; a black triangle indicates the location of the knickpoints caused by normal faulting of the HPF; grey triangles indicate the location of non-faulting knickpoints; numbers indicate the height of the knickpoint.

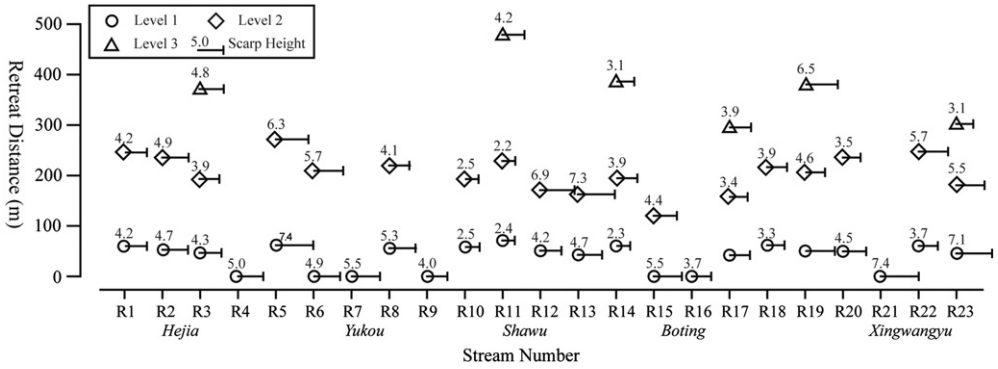

Fig. 10. Retreat distance of knickpoints from the HPF. "Rx" is the stream number. Villages near the streams are named below the stream numbers.

distance of 54.4 m from the HPF, the next most recent set of knickpoints (level 2) retreated 150–250 m upstream with a mean distance of 210.6 m, and the level 3 knickpoints retreated 300–500 m with a mean distance of 366.1 m. For these knickpoints, we measured the along-stream distances from the knickpoints to the intersections of each stream with the HPF. Additionally, the upstream drainage areas from the intersections of streams with the HPF were calculated. These reaches have a narrow range of area from 0.1 to 1.0 km^2 (Table 1). We plotted the knickpoints by their retreat distance (Fig. 10), but there are no obvious clusters in the distributions of retreat distances for all levels of knickpoints, and especially for levels 2 and 3.

6. Discussion

6.1. Knickpoint retreat

Knickpoint retreat has been both modelled (Howard et al., 1994; Whipple and Tucker, 1999) and simulated in flume experiments (Gardner, 1983; Frankel et al., 2007). Field-based data have also confirmed knickpoint retreat (Bishop et al, 2005; Crosby and Whipple, 2006; Castillo et al., 2013). Empirical models point to drainage area, a proxy for discharge, as a key control on knickpoint retreat rates for bedrock channel incision (Bishop et al., 2005; Crosby and Whipple, 2006). We attempted to validate the knickpoints in our study using the relationship between retreat distance and upstream drainage area. While the threshold drainage area at which a knickpoint is able to retreat is still in debate (Crosby and Whipple, 2006; Castillo et al., 2013), our observations show that many knickpoints are found in streams with drainage areas ranging from 0.1–1 km^2. These knickpoints slowly retreat upstream within these small drainage areas where the transition from fluvial-dominated to a debris flow-dominated erosion process occurs (Montgomery and Foufoula-Georgiou, 1993; Whipple, 2004; Wobus et al., 2006). It is possible that a knickpoint with a drainage area <1 km^2 in the HPF could retreat upstream once it was generated by an earthquake, and it is also possible that a knickpoint series could be developed by multiple earthquakes in a stream that crosses the fault. The distance a knickpoint retreats is not only dependent upon stream discharge, sediment supply, and substrate erodibility (Loget and van den Driessche, 2009), but it has been observed empirically that the retreat distance of a knickpoint increases exponentially as drainage area increases, following a power law function across a wide range of observed drainage areas (Kirby and Whipple, 2001; Bishop et al, 2005). We plotted the retreat distance of the most recent knickpoint versus the drainage area from which the knickpoints started

Table 1
Statistics of distance between the knickpoint and the fault, and the height of the knickpoint scarp.

No.	The number of knickpoints	Level 1		Level 2		Level 3		Drainage area (km^2)[a]	Class
		Recession distance (m)	Height (m)	Recession distance (m)	Height (m)	Recession distance (m)	Height (m)		
R1	2	59.9	4.2	245.8	4.2			0.304	III
R2	2	52.7	4.7	235.5	4.9			0.285	III
R3	3	46.6	4.3	193.2	3.9	371.5	4.8	0.133	III
R4	1	0	5						I
R5	2	61.9	7.4	282.6	6.3			0.463	III
R6	2	0	4.9	209.4	5.7				II
R7	1	0	5.5						I
R8	2	55.7	5.3	219.7	4.1			0.221	III
R9	1	0	4						I
R10	2	58.2	2.5	192	2.5			0.333	III
R11	3	71.1	2.4	228.9	2.2	478.9	4.2	0.803	III
R12	2	50.9	4.2	171	6.9			0.216	III
R13	2	42.7	4.7	162.6	7.3			0.133	III
R14	3	60.4	2.3	194.6	3.9	386.2	3.1	0.323	III
R15	2	0	5.5	120.1	4.4				II
R16	1	0	3.7						I
R17	3	42.1	3.9	157.6	3.4	283.1	3.9	0.075	III
R18	2	61.8	3.3	216.5	3.9			0.332	III
R19	2	50.3	5.6	206.3	4.6	375	6.5	0.117	III
R20	2	49.7	4.5	235.7	3.5			0.127	III
R21	1	0	7.4						I
R22	2	60.5	3.7	247.4	5.7			0.357	III
R23	3	45.6	7.1	180.7	5.5	302.1	3.1	0.256	III

[a] Drainage area was calculated at the intersections of reaches and the HPF, that is, at the position where the knickpoints started to propagate.

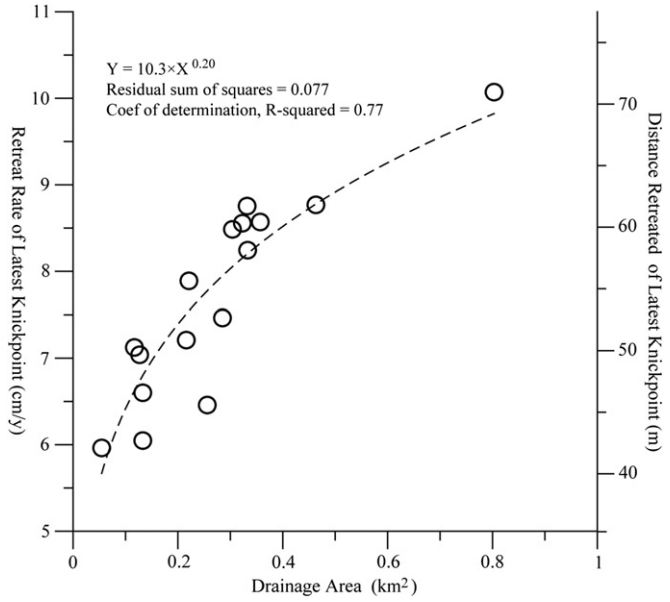

Fig. 11. Plot of knickpoint retreat rate (left vertical axis) and retreat distance from the fault (right vertical axis) versus drainage area. The tight correlation confirms the relationship between knickpoint retreat and drainage area in small bedrock channels. Circles denote observed knickpoints. The dashed line is the regression line, which follows a power law function.

to propagate, and a good exponential correlation was observed (Fig. 11, right vertical axis). This relationship confirms that the retreat distances of these knickpoints are reasonable.

Retreat rates of knickpoints can be calculated by dividing the retreat distance by the age of initiation. It is relatively easy to calculate the rate for the most recent knickpoint. Given that the most recent knickpoints (level 1) were generated in the 1303 earthquake, a retreat rate for every channel can be calculated by Eq. (1) using the migration distance and the elapsed time since the 1303 earthquake, that is, 706 years (the acquisition of IRS-P5 was in 2009). Because there is a linear relationship between the retreat distance and the retreat rate, the retreat rate for every channel also scales to its corresponding drainage area as a power law function (Fig. 11, left vertical axis), which has been observed in other transient landscapes (Hayakawa and Matsukura, 2003; Bishop et al., 2005).

6.2. Paleoearthquakes identified by normalised knickpoints

As mentioned in Section 4.1, we hypothesise that knickpoints maintain a constant retreat rate for a given channel. Therefore, the retreat distance of other knickpoints can be normalised to their respective formation time with Eq. (2), and using the retreat rate in each channel. If knickpoints in the channels that cross the HPF were related to the surface rupture caused by an earthquake, then these knickpoints after normalisation should be clustered around a similar formation time. We calculated the formation times of all knickpoints using their retreat distances and dividing by the retreat rates of the most recent knickpoints in the same reach. Fig. 12 shows obvious clustering of formation times of normalised knickpoints, and each cluster of formation times indicates the date of a corresponding earthquake. The subset including the most recent knickpoint defines the 1303 earthquake event, with a formation age of 706 a BP; the second subset includes 16 knickpoints, and defines the older earthquake event, with a formation age of 2269 to 3336 a BP; the third subset, despite sparser data, clearly defines the oldest event, with a formation age from 4504 to 5618 a BP.

To quantitatively define the age of knickpoint-generating paleoseismic events, we estimated the ages of the two earlier earthquake events by fitting the normalised knickpoint ages to a normal distribution. The result of this shows that the best fit earthquake ages with a 95% confidence interval are 2710 ± 102 and 4980 ± 646 a BP. Combining the most recent earthquake of 706 a BP with these two paleoearthquakes, we deduced that the recurrence interval of large earthquakes on the HPF is approximately 2000 years.

Paleoseismic analyses show that there were multiple surface-rupturing earthquakes on the HPF during the Holocene. Xiwei et al. (1993) demonstrated that other than the Hongdong Earthquake of 1303, two paleoearthquakes occurred on the HPF, dated at 2555–3475 a BP and at 4620–5455 a BP, respectively. Recently, other researchers arrived at similar conclusions: that the average recurrence interval for surface faulting events on the HPF is 1500–2000 years (Wali et al., 2004). Our paleoseismic results, demonstrated via normalised knickpoint retreat, are consistent with other paleoseismic studies both in the timing of events and the recurrence intervals.

The paleoseismic observations above are based on the condition that knickpoints maintain a constant rate of upstream migration. In reality, the retreat rate of a knickpoint would be affected by climatic changes as well as the drainage area. Climate studies have suggested that the climate in mid-eastern China has been becoming more cool and dry for the last 5 ka (Ke-Zhen, 1973; Ting-ru, 1983), and the decreased precipitation likely has reduced the retreat rates of knickpoints in the region. As a result, the ages of older knickpoints may be somewhat overestimated when they are calculated using the retreat rate of the knickpoints generated by the 1303 CE earthquake. In spite of the likely error in knickpoint age using a stable retreat rate, the earthquake record derived from normalised knickpoints seems reasonable when compared with other paleoseismic studies.

6.3. Coseismic vertical displacements generated by earthquakes

Given that normal faulting caused the knickpoints discussed in this paper, the height of the knickpoints may be related to the coseismic vertical displacement generated by earthquakes. For this reason we focused much of our attention on the height of knickpoints (e.g. Hayakawa and Oguchi, 2006, 2009), and used it as a proxy for the coseismic vertical displacement generated by earthquakes.

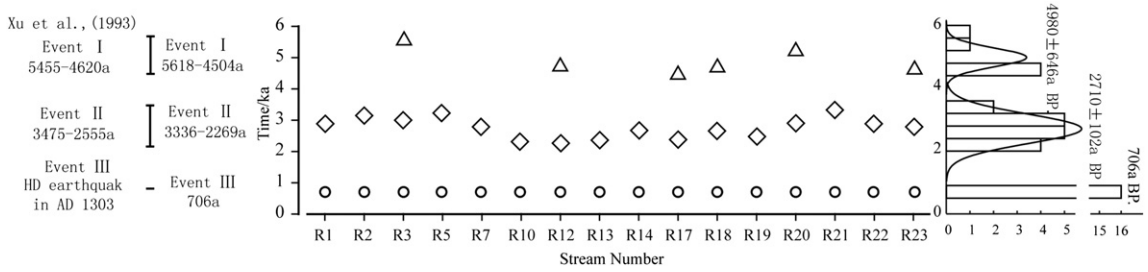

Fig. 12. Distribution of knickpoints after normalisation by the retreat rate of the most recent knickpoint (middle); faulting series estimated based on the knickpoint series (left); the histograms of normalised knickpoints for each level, the black curve is the normal distribution, and numbers are the best estimated values of the formation date of knickpoints, with a 95% confidence interval. Circles stand for knickpoints of level 1; diamonds stand for knickpoints of level 2; and triangles stand for knickpoints of level 3.

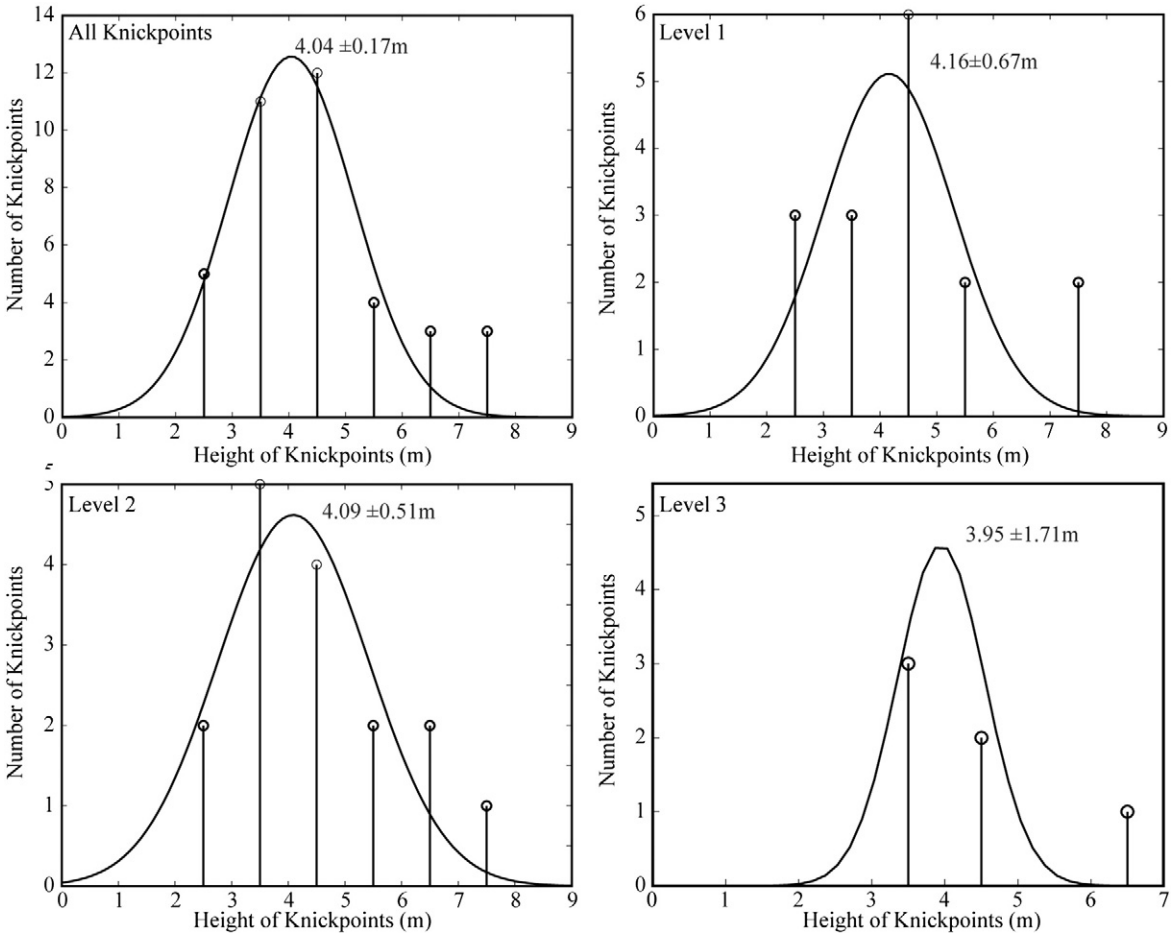

Fig. 13. Histograms of knickpoint heights for the entire set and each level. Blue curves are the normal distribution fit lines, and numbers indicate the best estimated values of knickpoint height with a 95% confidence interval.

We performed statistical analyses on the heights of knickpoints for the entire set and each level. Regardless of whether we examined the entire set or individual levels (1 to 3), the histograms show that the distributions of heights have a strikingly normal distribution. By fitting them to a normal distribution, the best estimations of heights are 4.04 ± 0.17, 4.16 ± 0.67, 4.09 ± 0.51 and 3.95 ± 1.71 m for the entire set, level 1, level 2, and level 3 respectively (Fig. 13). This suggests that the knickpoints preserve their original heights while they retreat upstream.

Coseismic displacements from earthquakes are important in assessing the seismic hazard of an active fault and for identifying earthquake recurrence patterns in the paleoseismic record (Zielke et al., 2010, 2012; Klinger et al., 2011). We questioned whether or not the height of knickpoints represents the coseismic vertical displacements of individual earthquakes. It has been observed in the field and in experiments that two migration models of knickpoints can be used to describe the behaviour of propagating knickpoints (Howard et al., 1994). In one model bedrock erosion is proportional to channel bed shear stress, and knickpoints rotate as they propagate upstream, diffusing away; in the other model, bedrock erosion is proportional to stream power, and knickpoints are broadly maintained as they propagate upstream, retreating in a parallel manner (Gardner, 1983; Whipple and Tucker, 1999; Crosby and Whipple, 2006). In the first model, the length of the knickpoint increases and the gradient of the knickpoint decreases as the knickpoint propagates upstream, whereas in the second model, the knickpoint morphology is usually steep and is maintained during propagation, and drainage area is the dominant controlling factor in knickpoint propagation. Most of the knickpoints that we identified along the HPF have steep faces (Fig. 3) and similar morphology (Fig. 9). It appears that the drainage area upstream provides the main influence for knickpoint retreat (Fig. 11). Therefore, we think that the knickpoints caused by normal faulting along the HPF obey the second model, and their morphology was maintained during their propagation. Similar results were observed after the 1999 Chi-Chi earthquake in West-Central Taiwan, where fluvial erosional processes tended to preserve and translate the morphology of fault-scarp knickpoints upstream, often referred to as a local scarp in the river reach (Sklar et al., 2005; Hayakawa et al., 2010). We speculate that the height of the knickpoints in the Huoshan Mountains represents the coseismic vertical displacement from earthquakes along the HPF.

If indeed the height of knickpoints and the coseismic vertical displacements from the HPF are similar, then the two older earthquakes produced fault vertical displacements of approximately 4 m, similar to that of the 1303 earthquake (Fig. 13). Other studies of repeated fault rupture confirm that some faults have exhibited a "characteristic" behaviour for multiple large earthquakes, that is, the magnitude, distribution, and style of slip on the fault have repeated during two or more consecutive events (Sieh, 1996). Klinger et al. (2011) showed a characteristic slip behaviour on the Fuyun fault, China, using analysis of coseismic displacements for successive earthquakes. As the vertical displacements are similar during the three successive earthquakes, we can conclude that the ruptures on the HPF obey a characteristic slip model. Based on the average displacement (4.04 ± 0.17 m), an expected moment magnitude $M_w = 7.5$ can be assigned to the HPF, using the equation linking displacement with moment magnitude for normal fault earthquakes described by Wells and Coppersmith (1994), consistent with the magnitude $M_s = 8.0$ derived from seismological data.

7. Conclusions

The results derived from a study of knickpoint distributions reveal two paleo-earthquakes in the Huoshan Piedmont Fault (HPF) and demonstrate that knickpoint locations can be exploited for paleoseismic investigations. A number of knickpoints are identified using high-resolution DEMs and the stream-gradient method (Hayakawa and Oguchi, 2006, 2009) in upper bedrock reaches of streams that cross the HPF. After excluding non-faulting knickpoints, 47 knickpoints were identified in 23 streams that cross the HPF. Analysis of the most recent knickpoints caused by the 1303 CE Hongdong Earthquake allows for local calibration of retreat rates. Application of these retreat rates towards estimating the formation dates of other knickpoints constrains the age ranges of the two knickpoint groups to be 2269–3336 a BP and 4504–5618 a BP, and yields a best estimated date of two paleoseismic events that occurred at 2710 ± 102 a BP and 4980 ± 646 a BP with a 95% confidence interval.

The knickpoints along the HPF obey the parallel retreating model in which knickpoint morphology was broadly maintained during propagation. The heights of knickpoints along the HPF represent the coseismic vertical displacements generated by the earthquakes that produced these knickpoints. Finally, large earthquakes along the HPF obey a characteristic slip model and typically have vertical offsets of approximately 4 m.

Acknowledgments

The authors would like to thank Prof. Arrowsmith, J R. for discussions in paleoseismological Analysis. Special thanks to Miguel Castillo and to Zhou Lin for helpful suggestions and comments that substantially improved this paper. We also thank Ian Pierce from the University of Nevada, Reno for his help in English writing. This research was supported by the National Natural Science Foundation of China (grant number: 41302173, 41372210) and Basic Research Fund from Institute of Geology, China Earthquake Administration (grant number: IGCEA1113).

References

Andrews, D.J., Hanks, T.C., 1985. Scarp degraded by linear diffusion: inverse solution for age. J. Geophys. Res. 90 (B12), 10193–10208.
Arrowsmith, J.R., Zielke, O., 2009. Tectonic geomorphology of the San Andreas Fault zone from high resolution topography: an example from the Cholame segment. Geomorphology 113 (1), 70–81. http://dx.doi.org/10.1016/j.geomorph.2009.01.002.
Arrowsmith, J.R., Rhodes, D.D., Pollard, D.D., 1998. Morphologic dating of scarps formed by repeated slip events along the San Andreas Fault, Carrizo Plain, California. J. Geophys. Res. 103, 10141–10160.
Attal, M., Cowie, P.A., Whittaker, A.C., Hobley, D., Tucker, G.E., Roberts, G.P., 2011. Testing fluvial erosion models using the transient response of bedrock rivers to tectonic forcing in the Apennines Italy. J. Geophys. Res. 116. http://dx.doi.org/10.1029/2010JF001875 F02005.
Bishop, P., Hoey, T.B., Jansen, J.D., Artza, I.L., 2005. Knickpoint recession rate and catchment area: the case of uplifted rivers in Eastern Scotland. Earth Surf. Process. Landf. 30, 767–778.
Burbank, D.W., Anderson, R.S., 2001. Tectonic Geomorphology. Blackwell Science, Massachusetts p. 274.
Castillo, M., Bishop, P., Jansen, J.D., 2013. Knickpoint retreat and transient bedrock channel morphology triggered by base-level fall in small bedrock river catchments: the case of the Isle of Jura, Scotland. Geomorphology 180, 1–9.
Crosby, B.T., Whipple, K.X., 2006. Knickpoint initiation and distribution within fluvial networks: 236 waterfalls in the Waipaoa River, North Island, New Zealand. Geomorphology 82, 16–38.
Deng, Q.D., Xu, X.W., 1994. Studies on the surface rupture zone of 1303 Hongdong earthquake of M = 8 and paleoearthquakes of Huoshan Fault in Shanxi Province. Earthq. Res. China 8 (2), 231–245.
Deng, Q.D., Cheng, S.P., Min, W., 1999. Discussion on Cenozoic tectonics and dynamics of Ordos block. J. Geomech. 5 (3), 13–21.
Duvall, A., Kirby, E., Burbank, D., 2004. Tectonic and lithologic controls on bedrock channel profiles and processes in coastal California. J. Geophys. Res. 109. http://dx.doi.org/10.1029/2003JF000086.
Foster, M.A., Kelsey, H.M., 2012. Knickpoint and knickzone formation and propagation, South Fork Eel River, northern California. Geosphere 8 (2), 403–416.
Frankel, K.L., Pazzaglia, F.J., Vaughn, J.D., 2007. Knickpoint evolution in a vertically bedded substrate, upstream-dipping terraces, and Atlantic slope bedrock channels. Geol. Soc. Am. Bull. 119, 476–486.
Gardner, T., 1983. Experimental study of knickpoint and longitudinal evolution in cohesive, homogeneous material. Geol. Soc. Am. Bull. 94, 664–672.
Giaccio, B., Galadini, F., Sposato, A., Messina, P., Moro, M., Zreda, M., Cittadini, A., Salvi, S., Todero, A., 2002. Image processing and roughness analysis of exposed bedrock fault planes as a tool for paleoseismological analysis: results from the Campo Felice fault (central Apennines, Italy). Geomorphology 49, 281–301.
Guo-an, Tang, Xuejun, Liu, Guonian, Lu, 2005. Principle and Method of Digital Elevation Model and Geoscience Analysis. Scence Press, Beijing.
Hayakawa, Y., Matsukura, Y., 2003. Recession rates of waterfalls in Boso Peninsula, Japan, and a predictive equation. Earth Surf. Process. Landf. 28, 675–684.
Hayakawa, Y.S., Oguchi, T., 2006. DEM-based identification of fluvial knickzones and its application to Japanese Mountain Rivers. Geomorphology 78, 90–106.
Hayakawa, Y.S., Oguchi, T., 2009. GIS analysis of fluvial knickzone distribution in Japanese mountain watersheds. Geomorphology 111 (1), 27–37.
Hayakawa, Yuichi S., Nobuhisa, Matsuta, Akira, Maekado, Yukinori, Matsukura, 2010. Decadal changes in fault-scarp knickpoints by bedrock erosion following 1999 Chi-Chi Earthquake in Taiwan. EGU Gen. Assem. 12 (EGU2010-3063-1, Abstracts).
Howard, A., Kerby, G., 1983. Channels changes in badlands. Geol. Soc. Am. Bull. 94, 739–752.
Howard, A.D., Dietrich, W.E., Seidl, M.A., 1994. Modeling fluvial erosion on regional to continental scales. J. Geophys. Res. Solid Earth 99 (B7), 13971–13986.
Jenson, S.K., Domingue, J.O., 1988. Extracting topographic structure from digital elevation data for geographic information system analysis. Photogramm. Eng. Remote. Sens. 54, 1593–1600.
Jijun, Li, 1988. Recent progress in the study on quaternary glaciations in China. J. Glaciol. Geocryol. 10 (3), 238–242 (in Chinese with English abstract).
Ke-Zhen, Zhu, 1973. Preliminary research on the climate change during the recent 5000 years in China. Sci. China 2, 1–22 (in Chinese).
Kirby, E., Whipple, K.X., 2001. Quantifying differential rock-uplift rates via stream profile analysis. Geology 29, 415–418. http://dx.doi.org/10.1130/0091-7613((2001)029<0415:QDRURV>2.0.CO;2).
Klinger, Y., Etchebes, M., Tapponnier, P., Narteau, C., 2011. Characteristic slip for five great earthquakes along the Fuyun fault in China. Nat. Geosci. 4 (6), 389–392. http://dx.doi.org/10.1038/ngeo1158.
Liping, Zhao, Fengde, Liu, Jian, Li, 2007. Preliminary research on position accuracy of IRS-P5. Remote. Sens. Appl. 2, 64–68 (in Chinese).
Liu-Zeng, J., Klinger, Y., Sieh, K., Rubin, C., Seitz, G., 2006. Serial ruptures of the San Andreas fault Carrizo Plain, California, revealed by three-dimensional excavations. J. Geophys. Res. 111. http://dx.doi.org/10.1029/2004JB003601.
Loget, N., van den Driessche, J., 2009. Wave train model for knickpoint migration. Geomorphology 106, 376–382.
McCalpin, J., 2009. Paleoseismology. Academic Press, San Diego, California, p. 629.
Ming-Chu, Chen, 2010. Knickpoint Retreat and Fluvial Incision Following The 1999 Chi-Chi Earthquake: Da-An River Gorge. Georgia Institute of Technology, a thesis of master degree, Taiwan.
Montgomery, D.R., Foufoula-Georgiou, E., 1993. Channel network source representation using digital elevation models. Water Resour. Res. 29 (12), 3925–3934. http://dx.doi.org/10.1029/93WR02463.
Nash, D.B., 1980. Morphological analysis of degraded normal fault scarps. J. Geol. 88, 353–360.
Qidang, Deng, Guihua, Yu, Wenhua, Ye, 1992. Relationship between earthquake magnitude and parameters of surface ruptures associated with historical earthquakes. In: Institute of geology SSB (Ed.), Research on Active Fault (2). Seismological Press, Beijing, pp. 247–264 (in Chinese).
Qidong, Deng, Yongkang, Ran, Xiaoping, Yang, Wei, Min, Chunyan, Qu, 2007. Map of Active Tectonics of China. Seismology Press, Beijing (in Chinese).
Righter, K., 1997. High bedrock incision rates in the Atenguillo River Valley, Jalisco, Western Mexico. Earth Surf. Process. Landf. 22, 337–343.
Scholz, C.H., 2002. The Mechanics of Earthquakes and Faulting. Second Ed. Cambridge U. Press, Cambridge, United Kingdom 471.
Sieh, K.E., 1978. Pre-historic large earthquakes produced by slip on the San Anderas fault at Pallett Creek, California. J. Geophys. Res. 83, 3907–3939.
Sieh, K., 1996. The repetition of large-earthquake ruptures. Proc. Natl. Acad. Sci. U. S. A. 93, 3764–3771.
Sieh, K., Jahns, R., 1984. Holocene activity of the San Andreas fault at Wallace Creek, California. Geol. Soc. Am. Bull. 95, 883–896. http://dx.doi.org/10.1130/0016-7606(1984)95<883:HAOTSA>2.0.CO;2.
Sklar, L.S., Stock, J.D., Roering, J.J., Kirchner, J.W., Dietrich, W.E., Chi, W., Hsu, L., Hsieh, M., Tsao, S., Chen, M., 2005. Evolution of Fault Scarp Knickpoints Following 1999 Chi-Chi Earthquake in West-central Taiwan. AGU Fall Meeting, Abstracts.
Snyder, N.P., Whipple, K.X., Tucker, G.E., Merritts, D.J., 2003. Channel response to tectonic forcing: field analysis of stream morphology and hydrology in the Mendocino triple junction region, northern California. Geomorphology 53, 97–127. http://dx.doi.org/10.1016/S0169-555X(02)00349-5.
Stewart, I., 1996. A rough guide to limestone fault scarps. J. Struct. Geol. 18 (10), 1259–1264.
Ting-ru, Zhou, 1983. Differentiation of Quaternary paleo-geographical environment in China. Sci. Geogr. Sin. 3, 3–18 (in Chinese).
Wali, Jiang, Qidong, Deng, Xiwei, Xu, 2004. Surface zone of the 1303 Hongdong M = 8 earthquake, Shanxi Province. Acta Seismol. Sin. 26 (4), 355–362 (in Chinese with English abstract).
Wallace, R.E., 1968. Notes on stream channels offset by the San Andreas Fault, southern Coast Ranges, California. In: Dickinson, W.R., Grantz, A. (Eds.), Conference on Geologic Problems of the San Andreas Fault System. Stanford University Publication in Geological Sciences, 11, pp. 6–21.
Wallace, R.E., 1981. Active Faults, Paleoseismology, and Earthquake Hazards in the Western United States. Simpson.

Wang, G.C., Cao, K., Zhang, K.X., Wang, A., Liu, C., Meng, Y.N., Xu, Y.D., 2011. Spatio-temporal Framework of Tectonic Uplift Stage of the Tibetan Plateau in Cenozoic. Science China, Earth Sciences, pp. 29–44.

Wells, D.L., Coppersmith, K.J., 1994. New empirical relationships among magnitude, rupture length, rupture width, rupture area, and surface displacement. Bull. Seismol. Soc. Am. 84, 974–1002.

Whipple, K.X., 2004. Bedrock rivers and the geomorphology of active orogens. Annu. Rev. Earth Planet. Sci. 32, 151–185.

Whipple, K.X., Tucker, G.E., 1999. Dynamics of the stream-power river incision model; implications for height limits of mountain ranges, landscape response timescales, and research needs. J. Geophys. Res. Solid Earth 104 (B8), 17661–17674.

Whittaker, A.C., Attal, M., Cowie, P.A., Tucker, G.E., Roberts, G.P., 2008. Decoding temporal and spatial patterns of fault uplift using transient river long profiles. Geomorphology 100, 506–526. http://dx.doi.org/10.1016/j.geomorph.2008.01.018.

Whittaker, A., Attal, M., Allen, P.A., 2010. Characterising the origin, nature and fate of sediment exported from catchments perturbed by active tectonics. Basin Res. 22, 809–828.

Wobus, C., Whipple, K.X., Kirby, E., Snyder, N., Johnson, J., Spyropolou, K., Crosby, B., Sheehan, D., 2006. Tectonics from topography: procedures, promise, and pitfalls. In: Willett, S.D., et al. (Eds.), Tectonics, Climate, and Landscape Evolution: Geological Society of America Special Paper. 398, pp. 55–74. http://dx.doi.org/10.1130/2006.2398(04).

Wohl, E.E., 1993. Bedrock channel incision along Piccaninny Creek, Australia. J. Geol. 101 (6), 749–761.

Xiwei, Xu., Qidong, Deng, 1990. The features of the Late Quaternary activity of the piedmont fault of Mt. Huoshan, Shanxi Province and 1303 Hongdong earthquake (Ms = 8). Seismol. Geol. 1, 21–30 (in Chinese with English abstract).

Xiwei, Xu., Qidong, Deng, Zhujun, Han, 1993. The late Quaternary activity of the piedmont fault of Mt. Huoshan and paleoearthquake study. In: Zongjin, Ma (Ed.), Earthquake Research and Systematical Disaster Reduction in Linfeng. Shanxi. Seismological Press, Beijing, pp. 136–148 (in Chinese with English abstract).

Xu, X.W., Ma, X.Y., 1992. Neotectonic activity along the Shanxi rift system, China. Tectonophysics 219, 305–325.

Yafeng, Shi, 1989. The Quaternary Glaciations and Environmental Variations in China. The Science Publishing Company, Beijing 7030007646.

Xu Yueren, Shen Xuhui, He Honglin, Chen Lize, Sun Haoyue, 2011. Application of CBERS-02B satellite images to Mt. Huoshan piedmont active fault mapping (1:50000 scale). China Science (F series), Supp., 202–212

Zhang, H.P., Zhang, P.Z., Fan, Q.C., 2011. Initiation and recession of the fluvial knickpoints: a case study from the Yalu River-Wangtian'e volcanic region, northeastern China. Sci. China Earth Sci. 54, 1746–1753. http://dx.doi.org/10.1007/s11430-011-4254-6.

Zielke, O., Arrowsmith, J.R., Grant-Ludwig, L., Akciz, S.O., 2010. Slip in the 1857 and earlier large earthquakes along the Carrizo Plain San Andreas fault. Science 327, 1119–1122. http://dx.doi.org/10.1126/science.1182781.

Zielke, O., Arrowsmith, J.R., Grant-Ludwig, L., Akciz, S.O., 2012. High-resolution topography-derived offsets along the 1857 Fort Tejon Earthquake Rupture Trace, San Andreas Fault. Bull. Seismol. Soc. Am. 102 (3), 1135–1154.